

A framework for self-supervised MR image reconstruction using sub-sampling via Noisier2Noise

Charles Millard and Mark Chiew

Abstract—In recent years, there has been attention on leveraging the statistical modeling capabilities of neural networks for reconstructing sub-sampled Magnetic Resonance Imaging (MRI) data. Most proposed methods assume the existence of a representative fully-sampled dataset and use fully-supervised training. However, for many applications, fully sampled training data is not available, and may be highly impractical to acquire. The development and understanding of self-supervised methods, which use only sub-sampled data for training, are therefore highly desirable. This work extends the Noisier2Noise framework, which was originally constructed for self-supervised denoising tasks, to variable density sub-sampled MRI data. We use the Noisier2Noise framework to analytically explain the performance of Self-Supervised Learning via Data Undersampling (SSDU), a recently proposed method that performs well in practice but until now lacked theoretical justification. We also use the framework to modify SSDU, which we find substantially improves its reconstruction quality and robustness, offering a test set mean-squared-error within 1% of fully supervised training on the fastMRI brain dataset.

Index Terms—Deep Learning, Image Reconstruction, Magnetic Resonance Imaging

I. INTRODUCTION

THE data acquisition process in Magnetic Resonance Imaging (MRI) consists of traversing a sequence of smooth paths through the Fourier representation of the image, referred to as “k-space”, which is inherently time-consuming. Images can be reconstructed from accelerated, sub-sampled acquisitions by leveraging the non-uniformity of receiver coil sensitivities, referred to as “parallel imaging” [1]–[4]. Compressed sensing [5], [6], which uses sparse models to reconstruct incoherently sampled data, has also been widely applied to MRI [7].

There has been significant research attention in recent years on methods that reconstruct sub-sampled MRI data with neural networks [8]–[19]. The majority of these works use fully-supervised training. To train a network in a fully-supervised

manner, there must be a dataset comprised of fully sampled k-space data $y_{0,t} \in \mathbb{C}^N$, where N is the dimension of k-space multiplied by the number of coils, and paired sub-sampled data $y_t = M_{\Omega_t} y_{0,t}$. Here, t indexes the training set and $M_{\Omega_t} \in \mathbb{R}^{N \times N}$ is a sub-sampling mask with sampling set Ω_t , so that the j th diagonal of M_{Ω_t} is 1 if $j \in \Omega_t$ and zero otherwise. Then a network f_θ with parameters θ is trained by seeking a minimum of a non-convex loss function:

$$\theta^* = \arg \min_{\theta} \sum_t L(f_\theta(y_t), y_{0,t}), \quad (1)$$

which could be, for example, an ℓ_p norm in the image domain after coil combination [20]. The network f_{θ^*} estimates the ground truth in the image domain or k-space depending on the choice of loss function. For a k-space to k-space network, $y_{0,s}$ can be estimated with $\hat{y}_s = f_{\theta^*}(y_s)$, where s indexes the test set. Alternatively, to ensure that all available data is used,

$$\hat{y}_s^{dc} = (\mathbb{1} - M_{\Omega_s}) f_{\theta^*}(y_s) + y_s \quad (2)$$

can be employed. Eqn. (2) overwrites all entries of $f_{\theta^*}(y_s)$ already sampled in y_s , so that the estimate is consistent with the acquired data; the superscript refers to “data consistent”.

Given sufficient representative training data, fully-supervised networks can yield substantial reconstruction quality gains over sparsity-based compressed sensing methods. There are a number of large datasets available for fully supervised training, such as the fastMRI knee and brain data [20]. However, for many contrasts, orientations, or regions of the anatomy of interest, fully sampled datasets are not publicly available. Fully sampled data is rarely acquired as part of a normal scanning protocol, so acquiring sufficient training data for a specific application is highly resource intensive. In some cases, it may not even be technically feasible to acquire such data [21]–[23]. Therefore, for MRI reconstruction with deep learning to be applicable to datasets acquired using only standard protocols, a training method that uses solely sub-sampled data is required.

There have been several attempts to train networks with only sub-sampled MRI data [24]–[31], some of which are based on methods from the denoising literature [32]–[38]. One such approach is Noise2Noise [32]. Rather than mapping y_t to $y_{0,t}$, Noise2Noise trains a network to map y_t to another sub-sampled k-space $y_T = M_{\Omega_T} y_{0,T}$ where Ω_T and Ω_t are independent and $y_{0,T} = y_{0,t}$ when $t = T$ [26]. A limitation of Noise2Noise is that it requires paired data, so the dataset must contain two independently sampled scans of the same

This work was supported in part by the by the Engineering and Physical Sciences Research Council, grant EP/T013133/1 and in part by the Royal Academy of Engineering, grant RF201617/16/23. The Wellcome Centre for Integrative Neuroimaging is supported by core funding from the Wellcome Trust, Grant/Award Number: 203139/Z/16/Z. The computational aspects of this research were supported by the Wellcome Trust Core Award Grant Number 203141/Z/16/Z and the NIHR Oxford BRC. The views expressed are those of the authors and not necessarily those of the NHS, the NIHR or the Department of Health.

Charles Millard and Mark Chiew are with the Wellcome Centre for Integrative Neuroimaging, FMRIB, Nuffield Department of Clinical Neurosciences, University of Oxford, Level 0, John Radcliffe Hospital, Oxford, OX3 9DU, UK. (email: charles.millard@ndcn.ox.ac.uk and mark.chiew@ndcn.ox.ac.uk)

k-space, which is not part of standard protocols. Further, any motion and phase drifts between scans would cause the paired data to be inconsistent, violating the central assumption that underlies the method.

Self-supervised learning via data undersampling (SSDU) [28] is a recently proposed method for ground-truth free training that does not require paired data. SSDU separates the sampling set Ω_t into two disjoint sets: $\Omega_t = A_t \cup B_t$ where $A_t \cap B_t = \emptyset$. Then the network is trained to recover $M_{A_t}y_t$ from $M_{B_t}y_t$.

$$\theta^* = \arg \min_{\theta} \sum_t L(M_{A_t}f_{\theta}(M_{B_t}y_t), M_{A_t}y_t), \quad (3)$$

At inference, the data consistent estimate

$$\hat{y}_s^{dc} = (\mathbf{1} - M_{\Omega_s})f_{\theta^*}(M_{B_s}y_s) + y_s \quad (4)$$

is used. SSDU was found to have a reconstruction quality comparable with fully supervised training given certain empirically selected choices of A_t and B_t . However, it was presented without theoretical justification. Although SSDU has similarities with Noise2Self [34], Noise2Self's analysis has a strong requirement on independent noise, so do not apply to k-space sampling in general.

This paper considers the recently proposed Noisier2Noise framework [35], which was originally constructed for denoising problems. We modify Noisier2Noise so that it can be applied to variable density sub-sampled data. To our knowledge, this is the first work that applies Noisier2Noise to image reconstruction. Like SSDU, the proposed modification of Noisier2Noise does not require paired data, and involves training a network to map from one subset of Ω_t to another. While SSDU recovers one disjoint set from the other, Noisier2Noise applies a second sub-sampling mask to the data, $\tilde{y}_t = M_{\Lambda_t}y_t = M_{\Lambda_t}M_{\Omega_t}y_{0,t}$, and the network is trained to recover y_t from \tilde{y}_t with an ℓ_2 loss. Then, during inference, the fully sampled data is estimated via a correction term based on the distributions of Λ_t and Ω_t that ensures that the estimate is correct in expectation.

Despite their superficial differences, we show that, in fact, SSDU and Noisier2Noise are closely related. Specifically, we demonstrate that SSDU is a version of Noisier2Noise with a particular loss function that removes the need for the correction term at inference. We use the mathematical tools developed for Noisier2Noise to prove that SSDU with an ℓ_2 loss correctly estimates fully sampled k-space in expectation. Further, we use Noisier2Noise to improve SSDU by suggesting an alternative procedure for splitting Ω_t into disjoint sets, which we find substantially improves its reconstruction quality and robustness.

Although this paper focuses on MRI reconstruction, we emphasize that none of the theoretical developments are specific to k-space. This framework is therefore applicable to any image reconstruction problem with a forward model that involves random sub-sampling, such as low dose x-ray computed tomography [39] or astronomical imaging [40].

II. THEORY

This section describes how the Noisier2Noise framework can be applied to sub-sampled data. Additive and multi-

plicative noise versions of Noisier2Noise are proposed in [35]. Based on the observation that a k-space sub-sampling mask can be considered as multiplicative “noise”, we extend Noisier2Noise to image reconstruction by modifying the latter. It is standard practice in MRI to sub-sample k-space with variable density, so that low frequencies, where the spectral density is larger, are sampled with higher probability [7]. Since the multiplicative noise version of standard Noisier2Noise assumes uniformity, this requires a modification of the framework to variable density sampling.

A. Variable density Noisier2Noise for reconstruction

The measurements $y_t = M_{\Omega_t}y_{0,t}$ can be considered as instances of random variables, which we denote as $Y = MY_0$. Now consider the multiplication of Y by a second mask \tilde{M} ,

$$\tilde{Y} = \tilde{M}Y = \tilde{M}MY_0,$$

so that \tilde{Y} is a further sub-sampled random variable. The following result states how the expectation of Y_0 can be computed from \tilde{Y} and Y .

Claim 1. *When $\mathbb{E}[M_{jj}] > 0$ for all j , the expectation of Y_0 given \tilde{Y} is*

$$\mathbb{E}[Y_0|\tilde{Y}] = (\mathbf{1} - K)^{-1}(\mathbb{E}[Y|\tilde{Y}] - K\tilde{Y}), \quad (5)$$

where K is a diagonal matrix defined as

$$K = (\mathbf{1} - \tilde{P}P)^{-1}(\mathbf{1} - P) \quad (6)$$

for $P = \mathbb{E}[M]$ and $\tilde{P} = \mathbb{E}[\tilde{M}]$.

Proof. See Appendix VI-A, which is based on the proof given in Section 3.4 of [35]. \square

Eqn. (5) generalizes the version of Noisier2Noise proposed for uniform, multiplicative noise in [35] to variable density sampling. The difference between the uniform and variable density versions is the matrix K , which is a scalar k in [35]. For the special case of uniform sub-sampling, P , \tilde{P} and therefore K are proportional to the identity matrix, and (5) simplifies to the uniform version.

Eqn. (5) implies that $\mathbb{E}[Y_0|\tilde{Y}]$ can be estimated without fully sampled data by training a network to estimate $\mathbb{E}[Y|\tilde{Y}]$. To do this, a network can be trained to minimize

$$\theta^* = \arg \min_{\theta} \mathbb{E}[\|W(f_{\theta}(\tilde{Y}) - Y)\|_2^2|\tilde{Y}] \quad (7)$$

for a full-rank matrix W . This minimization yields parameters that satisfy

$$\mathbb{E}[W^H W(f_{\theta^*}(\tilde{Y}) - Y)|\tilde{Y}] = 0.$$

If W is full-rank, $W^H W$ is also full rank, so

$$\mathbb{E}[f_{\theta^*}(\tilde{Y}) - Y|\tilde{Y}] = 0.$$

Using $\mathbb{E}[f_{\theta^*}(\tilde{Y})|\tilde{Y}] = f_{\theta^*}(\tilde{Y})$,

$$f_{\theta^*}(\tilde{Y}) = \mathbb{E}[Y|\tilde{Y}].$$

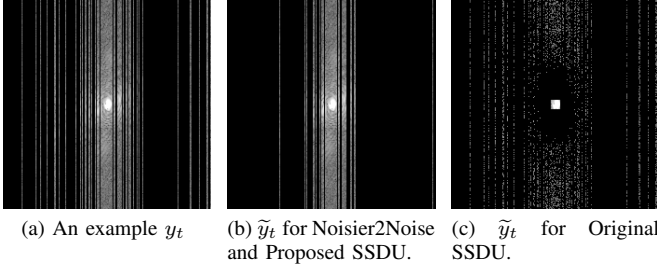


Fig. 1: An example of the singly sub-sampled k-space mask $y_t = M_{\Omega_t} y_{0,t}$, and doubly sub-sampled $\tilde{y}_t = M_{\Lambda_t} M_{\Omega_t} y_{0,t}$ with two approaches to generating Λ_t . Here, the acceleration factor of the first mask is $R = 4$ and the second is $\tilde{R} = 2$.

Therefore, by (5), a candidate for estimating fully sampled k-space without fully sampled data is

$$\mathbb{E}[Y_0 | \tilde{Y}] = (\mathbb{1} - K)^{-1} (f_{\theta^*}(\tilde{Y}) - K\tilde{Y})$$

This expression does not use Y , so does not use all available data. In practice, similarly to the fully supervised and SSDU versions stated in (2) and (4) respectively, we suggest instead using the data consistent version as the estimate of k-space,

$$\begin{aligned} \hat{Y}^{dc} &= (\mathbb{1} - M)\mathbb{E}[Y_0 | \tilde{Y}] + Y \\ &= (\mathbb{1} - M)(\mathbb{1} - K)^{-1} (f_{\theta^*}(\tilde{Y}) - K\tilde{Y}) + Y \\ &= (\mathbb{1} - M)(\mathbb{1} - K)^{-1} f_{\theta^*}(\tilde{Y}) + Y, \end{aligned}$$

where the final step uses $(\mathbb{1} - M)\tilde{Y} = (\mathbb{1} - M)\tilde{M}MY_0 = 0$.

This suggests the following procedure for training a network without fully-sampled data. For each sub-sampled k-space in the training set $y_t = M_{\Omega_t} y_{0,t}$, generate a further sub-sampled k-space $\tilde{y}_t = M_{\Lambda_t} y_t = M_{\Lambda_t} M_{\Omega_t} y_{0,t}$: see Fig. 1. Then, approximate (7) by training a network to minimize the loss function

$$\theta^* = \arg \min_{\theta} \sum_t \|W(f_{\theta}(\tilde{y}_t) - y_t)\|_2^2, \quad (8)$$

for some full-rank matrix W . During inference, estimate fully-sampled k-space with

$$\hat{y}_s^{dc} = (\mathbb{1} - M_{\Omega_s})(\mathbb{1} - K)^{-1} f_{\theta^*}(\tilde{y}_s) + y_s \quad (9)$$

where s indexes the test set.

In other words, we train a network to estimate the ‘‘singly’’ sub-sampled k-space y_t from ‘‘doubly’’ sub-sampled k-space \tilde{y}_t and then, during inference, apply a correction based on the diagonal matrix K to estimate the fully sampled data. The correction term only needs to be applied during inference and has minimal computational cost.

The mathematical requirement in Claim 1 that $\mathbb{E}[M_{jj}] > 0$ ensures that $(\mathbb{1} - K)$ is invertible. Intuitively, it is only possible for the network to learn to recover the j th k-space location if there is a non-zero probability that there are sampled examples of it in the training set. Noisier2Noise works because the network cannot deduce from \tilde{y}_t which entries of y_t are non-zero [35]. Therefore, the loss is minimized when the network learns to recover *all* of k-space.

In [35], only the version with $W = \mathbb{1}$ was presented. Here we present a version with non-trivial W for two reasons.

Firstly, we find that $W = (\mathbb{1} - K)^{-1}$, which compensates for the location-dependent sensitivity of the estimate, improves the performance of Noisier2Noise at inference: see Section IV. Secondly, it provides a link to SSDU; Section II-D shows that the Noisier2Noise framework with the rank-deficient $W = (\mathbb{1} - \tilde{M})M$ recovers SSDU exactly.

B. Choice of second mask

The only condition on the sampling masks for the proof of (5) is that $\mathbb{E}[M_{jj}] > 0$. The distribution of M is determined by the acquisition protocol. For the second mask \tilde{M} , following [35], we suggest using a distribution of \tilde{M} that matches the distribution of M , but not necessarily with the same parameters. One may be tempted to choose parameters so that the second mask only sub-samples by a small amount, so that the difference between \tilde{y}_t and y_t is small and $f_{\theta}(\tilde{y}_t)$ can be trained to higher accuracy. However, the j th diagonal of $(\mathbb{1} - K)^{-1}$, which we denote $(1 - k_j)^{-1}$, is very large when \tilde{p}_j is close to 1. Therefore, although $f_{\theta^*}(\tilde{y}_t)$ would recover y_t more accurately, (9) causes the estimate at inference to be very sensitive to inaccuracies. In other words, there is a trade-off between the accuracy of the network and the magnitude of the penalty at inference.

C. Choice of network

Noisier2Noise is agnostic to the network architecture. We have found that using the data consistent function

$$f_{\theta}(\tilde{y}_t) = (\mathbb{1} - M_{\Lambda_t} M_{\Omega_t}) g_{\theta}(\tilde{y}_t) + \tilde{y}_t, \quad (10)$$

where $g_{\theta}(\tilde{y}_t)$ is a network with arbitrary architecture, substantially improves the performance of Noisier2Noise compared with $f_{\theta}(\tilde{y}_t) = g_{\theta}(\tilde{y}_t)$. This is because (10) only recovers regions of k-space that are not already sampled in \tilde{y}_t , so $f_{\theta}(\tilde{y}_t)$ does not need to learn to map sampled k-space locations to themselves. Note that (10) ensures that $f_{\theta}(\tilde{y}_t)$ is consistent with \tilde{y}_t , while (9) ensures the estimate \hat{y}_s^{dc} is consistent with y_t , which is only applied at inference.

D. Relationship to SSDU

This section shows that SSDU [28] with an ℓ_2 loss is a version of Noisier2Noise with a particular rank-deficient choice of matrix W .

To see the connection between SSDU and Noisier2Noise, it is instructive to see the relationship between Noisier2Noise’s Λ_t and SSDU’s disjoint subsets A_t and B_t . Disjoint subsets of Ω_t can be formed in terms of Ω_t and Λ_t by setting $A_t = \Omega_t \setminus \Lambda_t$ and $B_t = \Omega_t \cap \Lambda_t$. The distribution of A_t and B_t are defined by the distributions of Ω_t and Λ_t and always satisfy $A_t \cup B_t = \Omega_t$ and $A_t \cap B_t = \emptyset$ as required. In terms of sampling masks, this is written as $M_{A_t} = (\mathbb{1} - M_{\Lambda_t})M_{\Omega_t}$ and $M_{B_t} = M_{\Lambda_t}M_{\Omega_t}$. Therefore, SSDU’s loss (11) with a squared ℓ_2 norm is

$$\begin{aligned} &\sum_t \|M_{A_t} f_{\theta}(M_{B_t} y_t) - M_{A_t} y_t\|_2^2 \\ &= \sum_t \|(\mathbb{1} - M_{\Lambda_t})M_{\Omega_t} (f_{\theta}(\tilde{y}_t) - y_t)\|_2^2 \quad (11) \end{aligned}$$

so is exactly Noisier2Noise with $W = (\mathbb{1} - \tilde{M})M$.

E. Proof of SSDU

This section shows that SSDU's weighting causes the correction $(\mathbf{1} - K)^{-1}$ at inference to no longer be necessary. When the weighting matrix is the random variable $W = (\mathbf{1} - \widetilde{M})M$, the network parameters are trained to seek a minimum of

$$\theta^* = \arg \min_{\theta} \mathbb{E}[\|(\mathbf{1} - \widetilde{M})M(f_{\theta}(\widetilde{Y}) - Y)\|_2^2 | \widetilde{Y}] \quad (12)$$

Unlike Noisier2Noise, $W = (\mathbf{1} - \widetilde{M})M$ is not full-rank, so $f_{\theta^*}(\widetilde{Y}) \neq \mathbb{E}[Y | \widetilde{Y}]$.

Claim 2. When $\mathbb{E}[M_{jj}] > 0$ for all j , a network with parameters that minimizes (12) satisfies

$$(\mathbf{1} - M\widetilde{M})f_{\theta^*}(\widetilde{Y}) = (\mathbf{1} - M\widetilde{M})\mathbb{E}[Y_0 | \widetilde{Y}].$$

Proof. See Appendix VI-B. \square

Therefore SSDU's k-space estimate is correct in expectation in regions of k-space that are not already sampled in \widetilde{Y} . This implies that it is crucial to use the data consistent estimate

$$\hat{Y}^{dc} = (\mathbf{1} - M)f_{\theta^*}(\widetilde{Y}) + Y, \quad (13)$$

as stated in (4), at inference.

We emphasize that unlike Noisier2Noise, SSDU does not require the correction term $(\mathbf{1} - K)^{-1}$ at inference. This implies that SSDU is less sensitive to inaccuracies in $f_{\theta^*}(\widetilde{Y})$, and we have found that SSDU outperforms Noisier2Noise in general when the same distributions of M and \widetilde{M} are used: see Section IV.

F. Understanding the need for correction

This section provides an intuitive explanation for why Noisier2Noise requires correction at inference but SSDU does not.

We can consider the ℓ_2 norm as a sum of contributions from three disjoint subsets of k-space: either $A_t = \Omega_t \cap \Lambda_t$, $B_t = \Omega_t \setminus \Lambda_t$ or $C_t = \Omega_t^c$, where Ω_t^c is the complement of Ω_t . Since $A_t \cup B_t \cup C_t = \{1, 2, \dots, N\}$, the ℓ_2 loss can be written as sum of contributions from A_t , B_t and C_t ,

$$\begin{aligned} & \|W(f_{\theta}(\widetilde{Y}) - Y)\|_2^2 \\ &= \|W(M\widetilde{M} + (\mathbf{1} - \widetilde{M})M + (\mathbf{1} - M))(f_{\theta}(\widetilde{Y}) - Y)\|_2^2. \end{aligned} \quad (14)$$

When f_{θ} has the data consistent form stated in (10), it follows that $M\widetilde{M}(f_{\theta}(\widetilde{Y}) - Y) = 0$. Then Noisier2Noise's loss can be written as

$$\begin{aligned} & \|W(f_{\theta}(\widetilde{Y}) - Y)\|_2^2 \\ &= \|W((\mathbf{1} - \widetilde{M})M + (\mathbf{1} - M))(f_{\theta}(\widetilde{Y}) - Y)\|_2^2 \\ &= \|W(\mathbf{1} - \widetilde{M})M(f_{\theta}(\widetilde{Y}) - Y)\|_2^2 + \|W(\mathbf{1} - M)f_{\theta}(\widetilde{Y})\|_2^2 \end{aligned} \quad (15)$$

where we have used $B_t \cap C_t = \emptyset$ to split the ℓ_2 norm and $(\mathbf{1} - M)Y = 0$ in the second term. Eqn. (15) is SSDU's loss function (11) plus a contribution from all $j \in \Omega_t^c$.

Intuitively, the second term on the right-hand-side of (15) causes the proposed method to underestimate regions of k-space with index $j \in \Omega_t^c$. This underestimation is compensated

for with $(\mathbf{1} - K)^{-1}$ at inference. For SSDU, where $W = (\mathbf{1} - \widetilde{M})M$, the second term on the right-hand-side of (15) is zero, k-space is not underestimated anywhere, and there is no need for a correction term at inference. The simpler choice $W = M$ would also remove the need for correction, and gives an identical loss function when the data consistent (10) is used.

III. EXPERIMENTAL METHOD

A. Description of data

We used the multi-coil brain data from the fastMRI dataset [20], which is comprised of fully sampled data. The reference fastMRI test set data is magnitude images only, without fully sampled k-space data. Since Noisier2Noise requires the k-space ℓ_2 loss, which we would also like to use at testing, phase is also required, so the suggested test set could not be used. We therefore discarded the data allocated for testing and generated our own partition in to training, validation and test sets. We only used data that was acquired on 16 coils, giving training, validation and test set sizes of 2020, 302, and 224 slices respectively.

B. Network architecture

For g_{θ} , we used the variant of the Variational Network (VarNet) [10] that estimates coil sensitivities on-the-fly [41], which performs competitively on the fastMRI leaderboard and is available as part of the fastMRI package¹. After a coil sensitivity estimation module, VarNet uses multiple repetitions of a module based on gradient descent, which is comprised of a data consistency term and a prior based on a U-net [42]. We used 6 repetitions of the main module, so that our model had around 1.5×10^7 parameters. We trained for 50 epochs using the Adam optimizer [43] with a learning rate of 10^{-3} in PyTorch.

C. Distribution of masks

So that the distribution of the sampling masks were known exactly, we generated our own masks rather than using those suggested in fastMRI. We chose a distribution of the first mask M so that columns of k-space were sampled. The central 10 columns were fully sampled and the remainder were sampled with polynomial variable density. We used polynomial order 8, and scaled the probability density so that it matched a desired acceleration factor. We ran each method with $R = 4, 8$, where $R = \mathbb{E}[1/\sum_j M_{jj}]$ is the expected acceleration factor. An example at $R = 4$ is shown in Fig. 1a.

In [35], it is suggested that the distribution of Noisier2Noise's second random variable is the same as the first, but not necessarily with the same distribution parameters. Therefore, for Noisier2Noise's second mask \widetilde{M} , we used the same distribution as M with a different scaling. An example with $R = 4$ and $\widetilde{R} = \mathbb{E}[1/\sum_j \widetilde{M}_{jj}] = 2$ is shown in Fig. 1b.

To ensure that k_j has non-zero denominator, we must use $\widetilde{p}_j < 1$ in the fully sampled central region of k-space, where $p_j = 1$. We set $\widetilde{p}_j = 1 - \epsilon$ in this region, where ϵ is a small

¹<https://github.com/facebookresearch/fastMRI>

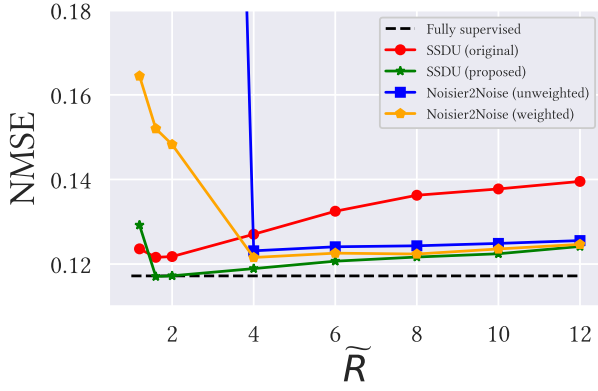


Fig. 2: The dependence of the test set NMSE on \tilde{R} at $R = 4$.

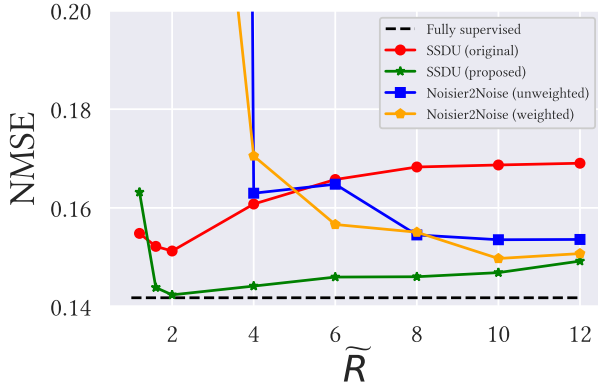


Fig. 3: The dependence of the test set NMSE on \tilde{R} at $R = 8$.

real constant. The data consistency step stated in (10) ensures that $f_{\theta}(\tilde{y}_t)$ does not change sampled inputs, so ϵ can be small without penalty. We used $\epsilon = 10^{-5}$.

In order to be a realistic simulation of prospectively subsampled data, the sampling set Ω_t must be fixed for all epochs. However, Λ_t need not be. Therefore, similar to the multi-mask SSDU approach proposed in [44], M_{Λ_t} was re-generated from the distribution of \tilde{M} once per epoch. Since the network sees more samples from the distribution of \tilde{M} , the loss function is closer to (7), so f_{θ^*} is expected to be a more accurate approximation of $\mathbb{E}[Y|\tilde{Y}]$. This has similarities with training data augmentation, as each slice is used to generate several inputs to the network.

D. Comparative methods

We trained Noisier2Noise using different variations of the ℓ_2 loss stated in (8). Firstly, we used $W = 1$, referred to as “Unweighted Noisier2Noise”. We also trained with $W = (1 - K)^{-1}$, referred to as “Weighted Noisier2Noise”. The weighted version anticipates the correction term applied at inference, optimizing for the vector transformed according to (9). Intuitively, the loss function compensates for the increased sensitivity to errors in regions of k-space with large $(1 - k_j)^{-1}$. This can also be interpreted as increasing the learning rate in regions of k-space where $(1 - k_j)^{-1}$ is large.

We also trained with $W = (1 - \tilde{M})M$ which, based on the relationship described in Section II-D, we refer to as “SSDU”,

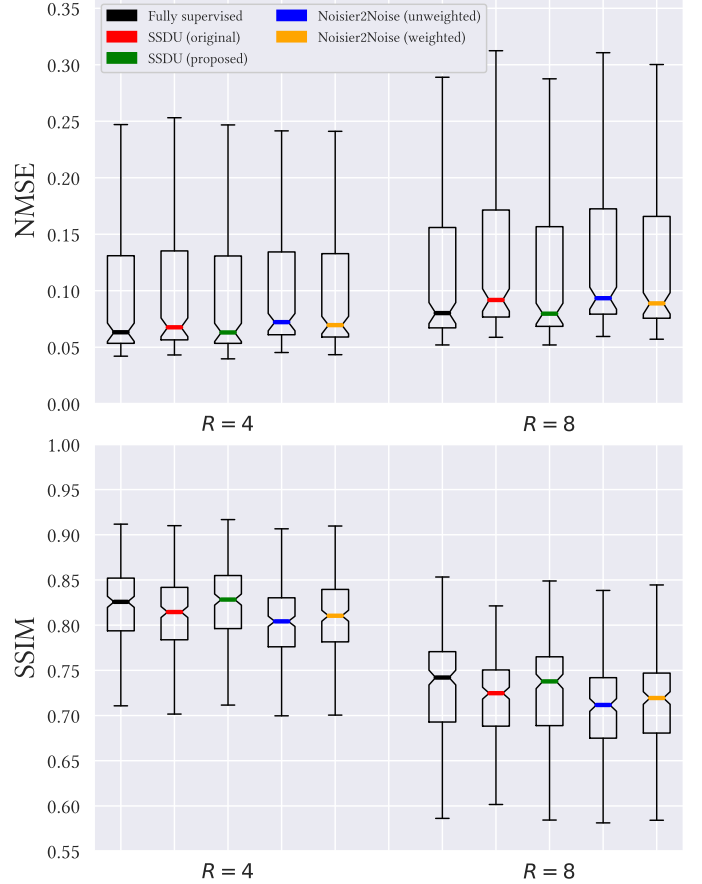


Fig. 4: The NMSE and SSIM for all methods at $R = 4, 8$, where \tilde{R} has been tuned to minimize the test set NMSE. Proposed SSDU was found to perform similarly to fully supervised training for both acceleration factors.

despite some differences between our implementation and [28]. In [28], a mixture of an ℓ_1 and ℓ_2 loss was used, whereas here, so that it can be fairly compared with Weighted and Unweighted Noisier2Noise, we used an ℓ_2 loss. The original SSDU, which is applied to a dataset with equidistant sampling of columns, suggests generating M_{B_t} with a fully sampled 10×10 central region and Bernoulli sampled with variable density in both dimensions otherwise, so that high frequencies are sampled with higher probability. We trained SSDU using a distribution of \tilde{M} of this type, referred to as “Original SSDU”, illustrated in Fig. 1c, and SSDU trained using the same distribution of \tilde{M} as M , referred to as “Proposed SSDU”, as in Fig. 1b. Like Noisier2Noise, M_{Λ_t} was re-generated once per epoch [44].

Finally, as a base-case target, we trained using a fully supervised method with an (unweighted) ℓ_2 loss. All methods had the same network architecture and training hyperparameters.

E. Quality metrics

To evaluate the reconstruction quality, we computed the NMSE in k-space on the test set. We also computed the image-

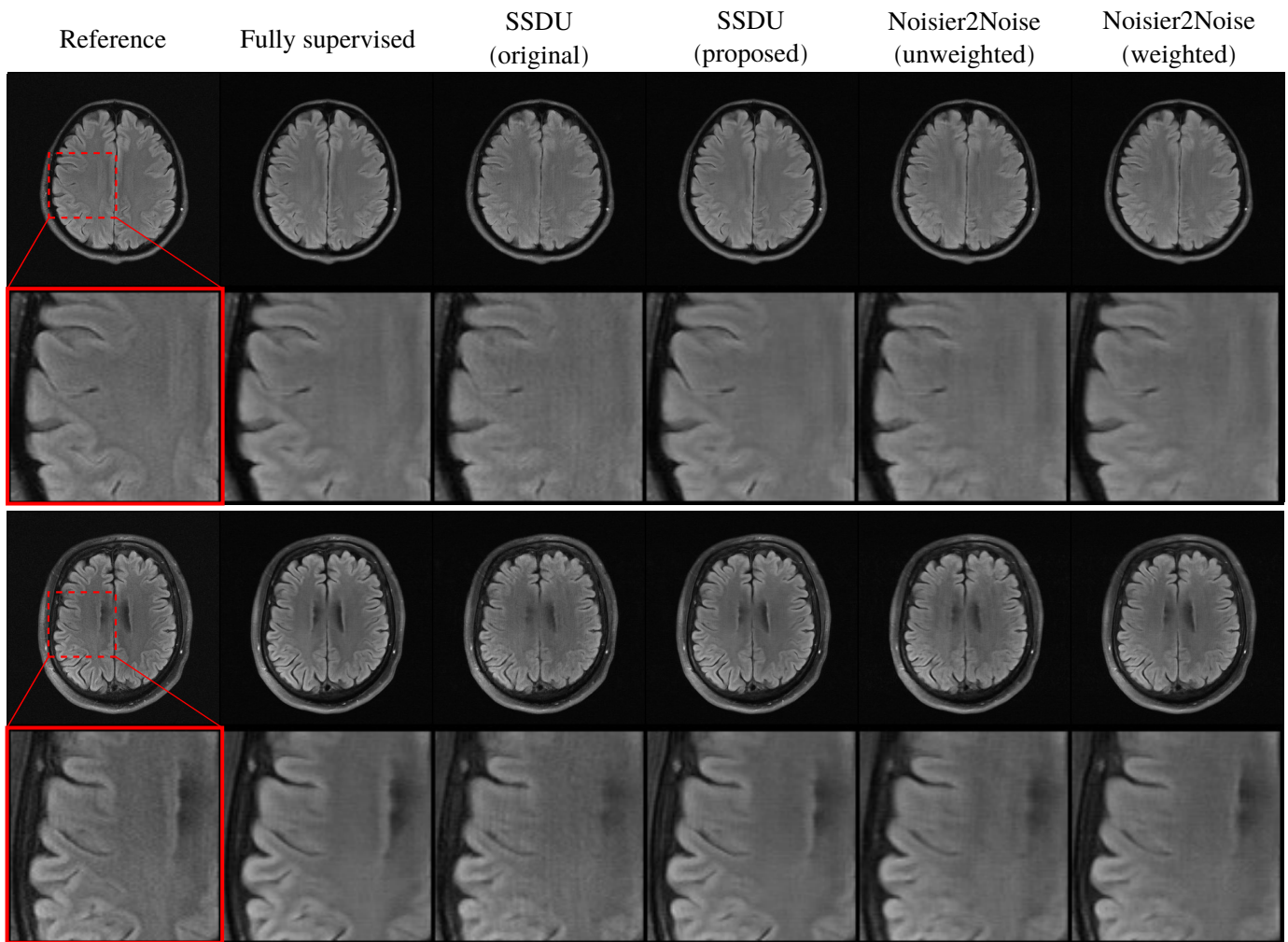


Fig. 5: Two reconstruction examples at $R = 4$, with a tuned \tilde{R} . The proposed variant of SSDU and Weighted Noisier2Noise perform competitively with fully supervised training, while Original SSDU and Unweighted Noisier2Noise exhibit streaking artifacts.

domain root-sum-of-squares (RSS), $\hat{x} = (\sum_c |F^H y_c|^2)^{1/2}$ where y_c is the k-space entries on coil c and F is the discrete Fourier transform, cropped the RSS estimate to a central 320×320 region and computed the Structural Similarity Index (SSIM) [45], as suggested in fastMRI [20].

IV. RESULTS AND DISCUSSION

We evaluated the dependence of Noisier2Noise and SSDU's performance on the distribution of \tilde{M} by varying the parameters such that \tilde{R} changed. We trained with \tilde{R} with values 1.2, 1.6 and between 2 and 12 in steps of 2. Figures 2 and 3 show the dependence of the mean test set NMSE on \tilde{R} for $R = 4$ and $R = 8$ respectively. Proposed SSDU yielded the best performance on the test set: with a tuned \tilde{R} , Proposed SSDU's NMSE was within 1% of fully supervised training.

Both Unweighted and Weighted Noisier2Noise's best performance was with $\tilde{R} = 4$ and $\tilde{R} = 10$ for $R = 4$ and $R = 8$ respectively. For \tilde{R} less than 4, the correction term is large, and Noisier2Noise performs poorly, especially for the unweighted variant. For instance, when $R = 8$ and $\tilde{R} = 2$, the maximum value of $(1 - k_j)^{-1}$, which is at the corner of k-space, is 141,

so is very sensitive to inaccuracies in this region. For larger \tilde{R} , the correction term is smaller and the reconstruction is less sensitive to errors, but there are fewer sampled locations in \tilde{y}_t so the network is less accurate. As \tilde{R} increases, the correction is smaller and Noisier2Noise's performance converges to that of Proposed SSDU. For instance, at $R = 4$, the performance on Noisier2Noise and Proposed SSDU is very similar at $\tilde{R} = 12$

Since SSDU does not need correction at inference, its optimal \tilde{R} is much lower: $\tilde{R} = 1.6$ and $\tilde{R} = 2$ for $R = 4$ and $R = 8$ respectively for both variants. For very low $\tilde{R} = 1.2$, SSDU does not perform well. This is because the doubly sub-sampled data is likely to be identical to the singly sub-sampled data, implying that the network trains very slowly. Original SSDU does not perform as well as fully supervised training for any \tilde{R} , consistent with the findings in Fig. 8 of [28]. Intuitively, Proposed SSDU gives better reconstruction quality because is not possible for the network to determine whether a zeroed k-space entry was masked by M_{Ω_t} or M_{Λ_t} , so minimizes its loss by learning to map to all of k-space. For Original SSDU, the location of the zeros of y_t can be deduced from \tilde{y}_t , so the network could learn to reconstruct columns sampled in

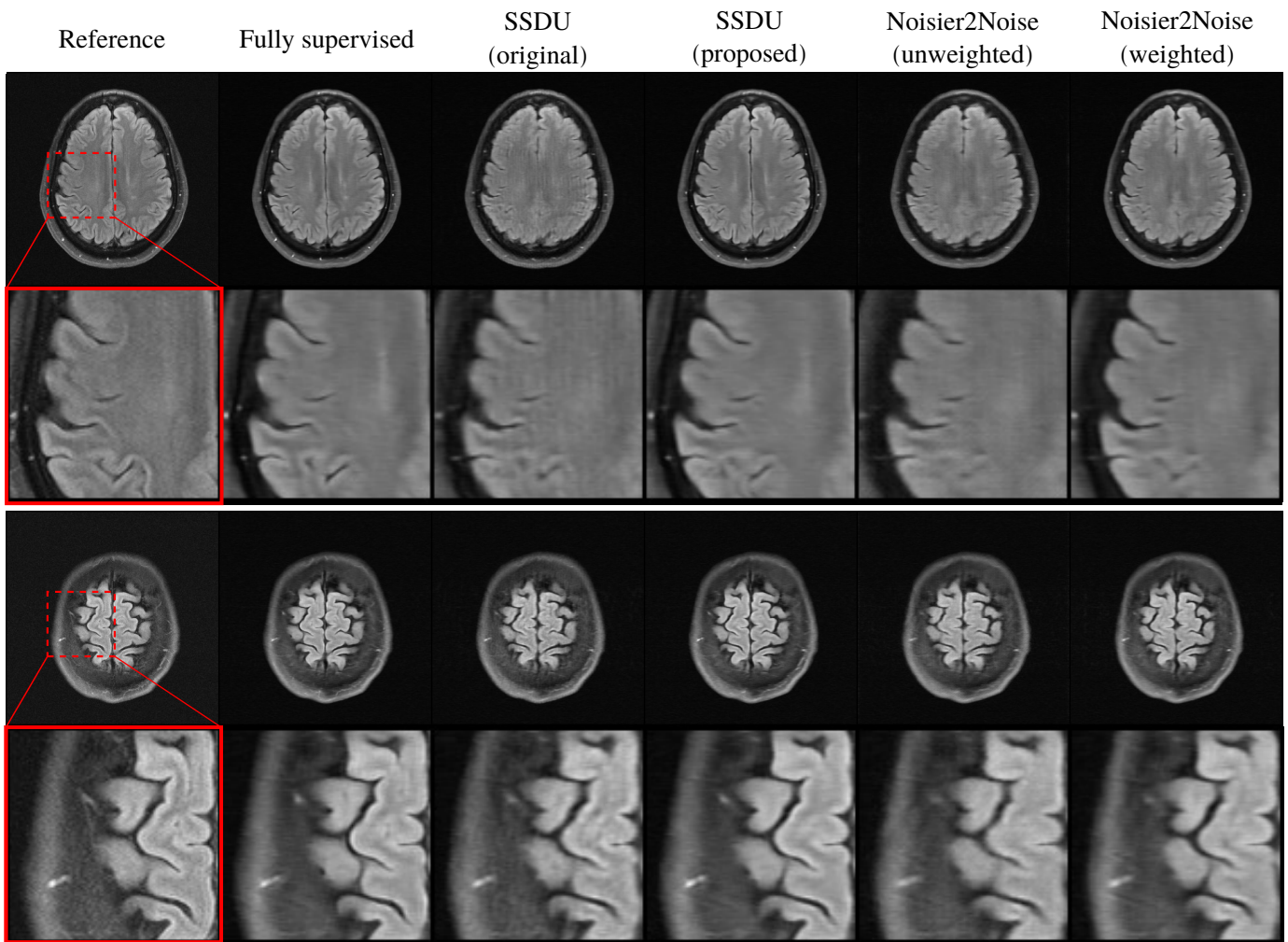


Fig. 6: Two reconstruction examples at $R = 8$, with a \tilde{R} tuned to minimize the test set NMSE.

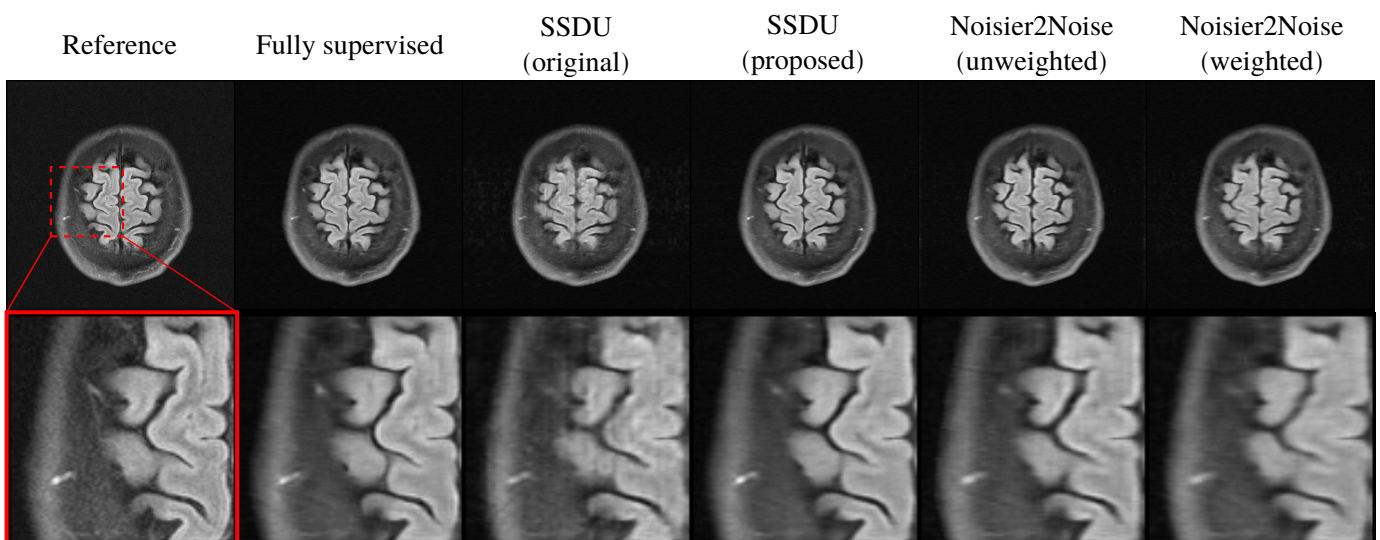


Fig. 7: The same slice from the second example in Fig. 6, but with \tilde{R} mistuned to be 2 higher than that which minimized the NMSE. Proposed SSDU is more robust than competing methods, continuing to performing comparably with fully supervised training.

y_t only. This suggests that, in general, better performance is possible when the distribution of the second mask is the same as the first, but not necessarily with the same parameters. Very recently, in [46], this was empirically observed for SSDU with spoke sampling.

Fig. 4 show box plots of the NMSE and SSIM of each method for $R = 4$ and $R = 8$ respectively, using the \tilde{R} that yielded the best test NMSE. The distribution of the NMSE and SSIM for Proposed SSDU is very similar to fully supervised training.

Fig. 5 shows two example RSS estimates from the test set at $R = 4$. Original SSDU and Unweighted Noisier2Noise suffer from streaking artifacts, while Original SSDU and Weighted Noisier2Noise perform similarly to fully supervised training. The difference between Proposed SSDU and the other methods is clearer in Fig. 6, which shows examples at $R = 8$. Here, Proposed SSDU is visibly sharper than competing self-supervised methods, especially at tissue boundaries.

Noisier2Noise's correction $(\mathbf{1} - K)^{-1}$ is only valid when an ℓ_2 loss is used; we have found that other loss functions do not perform well in practice. This loss leads to smoothing artifacts, even for fully supervised training, which are especially prominent at $R = 8$. For SSDU, since there is no correction term, loss functions other than ℓ_2 are possible. For instance, in [28], a mixture of ℓ_2 and ℓ_1 was used. Better visual quality may be achievable when SSDU is implemented with a different loss; we do not suggest using an ℓ_2 loss in general, it is only required here so that it can be compared fairly with Noisier2Noise.

Original SSDU was more sensitive to the tuning of \tilde{R} , with a relatively poor performance for $\tilde{R} \geq 4$. In contrast, Proposed SSDU performs reasonably well for the range of \tilde{R} explored, with only the very low $\tilde{R} = 1.2$ performing poorly. This is illustrated in Fig. 7, which shows the second $R = 8$ example in Fig. 6 but for when \tilde{R} is mistuned, so that $\tilde{R} = \tilde{R}_{opt} + 2$, where \tilde{R}_{opt} is the NMSE optimal choice. Visually, mistuned Proposed SSDU is still competitive with fully supervised training, while the competing methods show some degradation in image quality.

V. CONCLUSIONS AND FUTURE WORK

The proposed extension of Noisier2Noise to variable density sampled data yields reasonably high quality reconstructions from a neural network trained in a self supervised manner, without fully sampled data, with the weighted version slightly outperforming Original SSDU. Based on the observation that Noisier2Noise implies that the best performance is possible when the second mask is drawn from the same distribution as the first, we presented a variant of SSDU that outperforms Original SSDU and both Noisier2Noise variants, performing similarly to fully supervised training. We also found that Proposed SSDU was more robust to the choice of \tilde{R} than competing methods. Although the experimental work here focused on column sampling only, we emphasize that a similar improvement for any sampling scheme is expected, such as that recently found for spoke sampling in [46].

The theoretical analysis of SSDU presented in this paper applies to ℓ_2 loss functions only. Future work includes proving

SSDU for other loss functions, such as the mixed ℓ_1 - ℓ_2 loss used in [28].

In this work we aimed to recover fully sampled data, without explicitly attempting to remove measurement noise. Given a model of the measurement noise covariance, such a via an empty pre-scan, the additive and multiplicative noise versions of Noisier2Noise could be combined to simultaneously recover masked regions of k-space and denoise sampled regions [47].

VI. APPENDICES

A. Proof of variable density Noisier2Noise

This appendix proves that

$$\mathbb{E}[Y_0|\tilde{Y}] = (\mathbf{1} - K)^{-1}(\mathbb{E}[Y|\tilde{Y}] - K\tilde{Y}), \quad (16)$$

where $K = (\mathbf{1} - \tilde{P}P)^{-1}(\mathbf{1} - P)$ for $P = \mathbb{E}[M]$ and $\tilde{P} = \mathbb{E}[\tilde{M}]$.

Proof. This proof is based on Section 3.4 of Noisier2Noise [35], but with substantially more mathematical detail and generalized to variable density sampling. Following the convention from the compressed sensing literature, this paper uses p_j to refer to the probability that the j th location in k-space is sampled. This differs to [35], which uses p to denote the probability that a pixel is *zeroed*.

We wish to compute $\mathbb{E}[Y_j|\tilde{Y}_j]$ as a function of $\mathbb{E}[Y_{0,j}|\tilde{Y}_j]$. Since Y_j must not be masked for \tilde{Y}_j to be non-zero, $\mathbb{E}[Y_j|\tilde{Y}_j \neq 0] = \tilde{Y}_j$. The alternative is $\tilde{Y}_j = 0$. In this case, there are two possibilities, either $Y_j = 0$ or $Y_j \neq 0$:

$$\begin{aligned} \mathbb{E}[Y_j|\tilde{Y}_j = 0] &= \mathbb{E}[Y_j|\tilde{Y}_j = 0 \cap Y_j = 0]\mathbb{P}[Y_j = 0|\tilde{Y}_j = 0] \\ &\quad + \mathbb{E}[Y_j|\tilde{Y}_j = 0 \cap Y_j \neq 0]\mathbb{P}[Y_j \neq 0|\tilde{Y}_j = 0] \\ &= 0 \cdot k_j + \mathbb{E}[Y_j|\tilde{Y}_j = 0 \cap Y_j \neq 0] \cdot (1 - k_j) \end{aligned}$$

where we define $k_j = \mathbb{P}[Y_j = 0|\tilde{Y}_j = 0]$. Since $\mathbb{E}[Y_j|\tilde{Y}_j = 0 \cap Y_j \neq 0] = \mathbb{E}[Y_{0,j}]$, we can write

$$\mathbb{E}[Y_j|\tilde{Y}_j = 0] = \mathbb{E}[Y_{0,j}](1 - k_j).$$

Both the $\mathbb{E}[Y_j|\tilde{Y}_j = 0]$ and $\mathbb{E}[Y_j|\tilde{Y}_j \neq 0]$ cases can be encompassed with

$$\mathbb{E}[Y_j|\tilde{Y}_j] = (1 - k_j)\mathbb{E}[Y_{0,j}|\tilde{Y}_j] + k_j\tilde{Y}_j. \quad (17)$$

This expression can be verified by first considering $\tilde{Y}_j = 0$, giving $\mathbb{E}[Y_j|\tilde{Y}_j = 0] = \mathbb{E}[Y_{0,j}](1 - k_j)$ as required, and secondly setting $\tilde{Y}_j \neq 0$, giving $\mathbb{E}[Y_j|\tilde{Y}_j \neq 0] = \tilde{Y}_j$ as required. When $k_j \neq 1$ we can rearrange (17) for $\mathbb{E}[Y_{0,j}|\tilde{Y}_j]$,

$$\mathbb{E}[Y_{0,j}|\tilde{Y}_j] = (1 - k_j)^{-1}(\mathbb{E}[Y_j|\tilde{Y}_j] - k_j\tilde{Y}_j). \quad (18)$$

Now, we compute k_j :

$$k_j = \mathbb{P}[Y_j = 0|\tilde{Y}_j = 0] = \frac{\mathbb{P}[Y_j = 0 \cap \tilde{Y}_j = 0]}{\mathbb{P}[\tilde{Y}_j = 0]}$$

The numerator is

$$\begin{aligned} \mathbb{P}[Y_j = 0 \cap \tilde{Y}_j = 0] &= \mathbb{P}[Y_j = 0] \\ &= 1 - p_j, \end{aligned}$$

where $p_j = \mathbb{P}[Y_j \neq 0] = \mathbb{E}[M_{jj}]$ is the probability that $j \in \Omega$. The denominator is

$$\begin{aligned} \mathbb{P}[\tilde{Y}_j = 0] &= \mathbb{P}[\tilde{Y}_j = 0 | Y_j = 0] \mathbb{P}[Y_j = 0] \\ &\quad + \mathbb{P}[\tilde{Y}_j = 0 | Y_j \neq 0] \mathbb{P}[Y_j \neq 0] \\ &= 1 \cdot (1 - p_j) + (1 - \tilde{p}_j) p_j \\ &= 1 - \tilde{p}_j p_j \end{aligned}$$

where $\tilde{p}_j = \mathbb{P}[\tilde{Y} \neq 0] = \mathbb{E}[\tilde{M}_{jj}]$. Therefore

$$k_j = \mathbb{P}[Y_j = 0 | \tilde{Y}_j = 0] = \frac{1 - p_j}{1 - \tilde{p}_j p_j},$$

which implies that since $p_j > 0$ by assumption, $(1 - k_j)^{-1}$ exists. Writing (18) in terms of vector and matrix random variables yields (16), as required. \square

B. Proof of SSDU

This appendix proves Claim 2. The minimum of SSDU's loss function gives a function that satisfies

$$\mathbb{E}[(\mathbf{1} - \tilde{M})M(f_{\theta^*}(\tilde{Y}) - Y)|\tilde{Y}] = 0 \quad (19)$$

Claim 3. The left-hand-side of (19) is

$$\begin{aligned} \mathbb{E}[(\mathbf{1} - \tilde{M})M(f_{\theta^*}(\tilde{Y}) - Y)|\tilde{Y}] \\ = (\mathbf{1} - K)(\mathbf{1} - \tilde{M}M)(f_{\theta^*}(\tilde{Y}) - \mathbb{E}[Y_0|\tilde{Y}]) \end{aligned}$$

Proof. When $\tilde{Y}_j \neq 0$, $(1 - \tilde{m}_j)m_j = 0$ where \tilde{m}_j and m_j are the j th diagonals of \tilde{M} and M respectively, so

$$\mathbb{E}[(1 - \tilde{m}_j)m_j(f_{\theta^*}(\tilde{Y})_j - Y_j)|\tilde{Y}_j \neq 0] = 0$$

When $\tilde{Y}_j = 0$, $(1 - \tilde{m}_j)m_j = m_j$, so

$$\begin{aligned} \mathbb{E}[(1 - \tilde{m}_j)m_j(f_{\theta^*}(\tilde{Y})_j - Y_j)|\tilde{Y}_j = 0] \\ = \mathbb{E}[m_j(f_{\theta^*}(\tilde{Y})_j - Y_j)|\tilde{Y}_j = 0] \end{aligned}$$

We can use a similar approach to the derivation of (18),

$$\begin{aligned} \mathbb{E}[m_j(f_{\theta^*}(\tilde{Y})_j - Y_j)|\tilde{Y}_j = 0] \\ = \mathbb{E}[m_j(f_{\theta^*}(\tilde{Y})_j - Y_j)|\tilde{Y}_j = 0 \cap Y_j = 0] \mathbb{P}[Y_j = 0|\tilde{Y}_j = 0] \\ + \mathbb{E}[m_j(f_{\theta^*}(\tilde{Y})_j - Y_j)|\tilde{Y}_j = 0 \cap Y_j \neq 0] \mathbb{P}[Y_j \neq 0|\tilde{Y}_j = 0] \\ = 0 \cdot k_j + \mathbb{E}[(f_{\theta^*}(\tilde{Y})_j - Y_j)|\tilde{Y}_j = 0 \cap Y_j \neq 0] \cdot (1 - k_j) \\ = \mathbb{E}[(f_{\theta^*}(\tilde{Y})_j - Y_{0,j})|\tilde{Y}_j = 0 \cap Y_j \neq 0] \cdot (1 - k_j) \end{aligned}$$

The $\tilde{Y}_j \neq 0$ and $\tilde{Y}_j = 0$ cases can be encompassed with

$$\begin{aligned} \mathbb{E}[m_j(f_{\theta^*}(\tilde{Y})_j - Y_{0,j})|\tilde{Y}_j] \\ = (1 - k_j)(\mathbf{1} - \tilde{m}_j m_j) \mathbb{E}[(f_{\theta^*}(\tilde{Y})_j - Y_{0,j})|\tilde{Y}_j] \end{aligned}$$

Using the vector form of this result and setting $\mathbb{E}[f_{\theta^*}(\tilde{Y})|\tilde{Y}] = f_{\theta^*}(\tilde{Y})$ gives the required result. \square

Since $p_j > 0$ for all j by assumption, $(\mathbf{1} - K)$ is full rank, so (19) is

$$\begin{aligned} (\mathbf{1} - K)(\mathbf{1} - \tilde{M}M)(f_{\theta^*}(\tilde{Y}) - \mathbb{E}[Y_0|\tilde{Y}]) &= 0 \\ (\mathbf{1} - \tilde{M}M)(f_{\theta^*}(\tilde{Y}) - \mathbb{E}[Y_0|\tilde{Y}]) &= 0, \end{aligned}$$

which is equivalent to Claim 2.

REFERENCES

- [1] J. B. Ra and C. Y. Rim, "Fast imaging using subencoding data sets from multiple detectors," *Magnetic resonance in medicine*, vol. 30, no. 1, pp. 142–145, 1993.
- [2] K. P. Pruessmann, M. Weiger, M. B. Scheidegger, and P. Boesiger, "SENSE: Sensitivity encoding for fast MRI," *Magnetic resonance in medicine*, vol. 42, pp. 952–62, nov 1999.
- [3] M. A. Griswold, P. M. Jakob, R. M. Heidemann, M. Nittka, V. Jellus, J. Wang, B. Kiefer, and A. Haase, "Generalized autocalibrating partially parallel acquisitions (GRAPPA)," *Magnetic Resonance in Medicine*, vol. 47, pp. 1202–1210, jun 2002.
- [4] M. Uecker, P. Lai, M. J. Murphy, P. Virtue, M. Elad, J. M. Pauly, S. S. Vasanawala, and M. Lustig, "ESPIRiT—an eigenvalue approach to autocalibrating parallel MRI: Where SENSE meets GRAPPA," *Magnetic Resonance in Medicine*, vol. 71, pp. 990–1001, mar 2014.
- [5] D. L. Donoho, "Compressed sensing," *IEEE Transactions on Information Theory*, vol. 52, pp. 1289–1306, apr 2006.
- [6] E. Candes, J. Romberg, and T. Tao, "Robust uncertainty principles: exact signal reconstruction from highly incomplete frequency information," *IEEE Transactions on Information Theory*, vol. 52, pp. 489–509, feb 2006.
- [7] M. Lustig, D. Donoho, and J. M. Pauly, "Sparse MRI: The application of compressed sensing for rapid MR imaging," *Magnetic Resonance in Medicine*, vol. 58, pp. 1182–1195, dec 2007.
- [8] S. Wang, Z. Su, L. Ying, X. Peng, S. Zhu, F. Liang, D. Feng, and D. Liang, "Accelerating magnetic resonance imaging via deep learning," in *2016 IEEE 13th International Symposium on Biomedical Imaging (ISBI)*, pp. 514–517, IEEE, 2016.
- [9] K. Kwon, D. Kim, and H. Park, "A parallel MR imaging method using multilayer perceptron," *Medical physics*, vol. 44, no. 12, pp. 6209–6224, 2017.
- [10] K. Hammernik, T. Klatzer, E. Kobler, M. P. Recht, D. K. Sodickson, T. Pock, and F. Knoll, "Learning a variational network for reconstruction of accelerated MRI data," *Magnetic resonance in medicine*, vol. 79, no. 6, pp. 3055–3071, 2018.
- [11] A. P. Yazdanpanah, O. Afacan, and S. Warfield, "Deep Plug-and-Play Prior for Parallel MRI Reconstruction," in *2019 IEEE/CVF International Conference on Computer Vision Workshop (ICCVW)*, pp. 3952–3958, IEEE, 2019.
- [12] J. Liu, Y. Sun, C. Eldeniz, W. Gan, H. An, and U. S. Kamilov, "RARE: Image reconstruction using deep priors learned without groundtruth," *IEEE Journal of Selected Topics in Signal Processing*, vol. 14, no. 6, pp. 1088–1099, 2020.
- [13] Y. Yang, J. Sun, H. Li, and Z. Xu, "Deep ADMM-Net for compressive sensing MRI," in *Proceedings of the 30th international conference on neural information processing systems*, pp. 10–18, 2016.
- [14] Y. Yang, J. Sun, H. Li, and Z. Xu, "ADMM-CSNet: A deep learning approach for image compressive sensing," *IEEE transactions on pattern analysis and machine intelligence*, vol. 42, no. 3, pp. 521–538, 2018.
- [15] J. Zhang and B. Ghanem, "ISTA-Net: Interpretable optimization-inspired deep network for image compressive sensing," in *Proceedings of the IEEE conference on computer vision and pattern recognition*, pp. 1828–1837, 2018.
- [16] B. Zhu, J. Z. Liu, S. F. Cauley, B. R. Rosen, and M. S. Rosen, "Image reconstruction by domain-transform manifold learning," *Nature*, vol. 555, no. 7697, pp. 487–492, 2018.
- [17] T. M. Quan, T. Nguyen-Duc, and W.-K. Jeong, "Compressed sensing MRI reconstruction using a generative adversarial network with a cyclic loss," *IEEE transactions on medical imaging*, vol. 37, no. 6, pp. 1488–1497, 2018.
- [18] M. Mardani, E. Gong, J. Y. Cheng, S. S. Vasanawala, G. Zaharchuk, L. Xing, and J. M. Pauly, "Deep generative adversarial neural networks for compressive sensing MRI," *IEEE transactions on medical imaging*, vol. 38, no. 1, pp. 167–179, 2018.
- [19] R. Ahmad, C. A. Bouman, G. T. Buzzard, S. Chan, S. Liu, E. T. Reehorst, and P. Schniter, "Plug-and-Play Methods for Magnetic Resonance Imaging: Using Denoisers for Image Recovery," *IEEE Signal Processing Magazine*, vol. 37, pp. 105–116, jan 2020.
- [20] J. Zbontar, F. Knoll, A. Sriram, T. Murrell, Z. Huang, M. J. Muckley, A. Defazio, R. Stern, P. Johnson, M. Bruno, *et al.*, "fastMRI: An open dataset and benchmarks for accelerated MRI," *arXiv preprint arXiv:1811.08839*, 2018.
- [21] M. Uecker, S. Zhang, D. Voit, A. Karaus, K.-D. Merboldt, and J. Frahm, "Real-time MRI at a resolution of 20 ms," *NMR in Biomedicine*, vol. 23, no. 8, pp. 986–994, 2010.

- [22] H. Haji-Valizadeh, A. A. Rahsepar, J. D. Collins, E. Bassett, T. Isakova, T. Block, G. Adluru, E. V. DiBella, D. C. Lee, J. C. Carr, *et al.*, "Validation of highly accelerated real-time cardiac cine MRI with radial k-space sampling and compressed sensing in patients at 1.5 T and 3T," *Magnetic resonance in medicine*, vol. 79, no. 5, pp. 2745–2751, 2018.
- [23] Y. Lim, Y. Zhu, S. G. Lingala, D. Byrd, S. Narayanan, and K. S. Nayak, "3D dynamic MRI of the vocal tract during natural speech," *Magnetic resonance in medicine*, vol. 81, no. 3, pp. 1511–1520, 2019.
- [24] J. Yoo, K. H. Jin, H. Gupta, J. Yerly, M. Stuber, and M. Unser, "Time-Dependent Deep Image Prior for Dynamic MRI," *IEEE Transactions on Medical Imaging*, vol. 40, no. 12, pp. 3337–3348, 2021.
- [25] J. I. Tamir, X. Y. Stella, and M. Lustig, "Unsupervised deep basis pursuit: Learning reconstruction without ground-truth data," in *ISMRM annual meeting*, vol. 27, p. 0660, 2019.
- [26] P. Huang, C. Zhang, H. Li, S. K. Gaire, R. Liu, X. Zhang, X. Li, and L. Ying, "Deep MRI reconstruction without ground truth for training," in *Proceedings of 27th Annual Meeting of ISMRM*, 2019.
- [27] E. K. Cole, J. M. Pauly, S. S. Vasanawala, and F. Ong, "Unsupervised MRI reconstruction with generative adversarial networks," *arXiv preprint arXiv:2008.13065*, 2020.
- [28] B. Yaman, S. A. H. Hosseini, S. Moeller, J. Ellermann, K. Uğurbil, and M. Akçakaya, "Self-supervised learning of physics-guided reconstruction neural networks without fully sampled reference data," *Magnetic resonance in medicine*, vol. 84, no. 6, pp. 3172–3191, 2020.
- [29] S. Liu, P. Schniter, and R. Ahmad, "MRI Recovery with A Self-calibrated Denoiser," *arXiv preprint arXiv:2110.09418*, 2021.
- [30] H. K. Aggarwal, A. Pramanik, and M. Jacob, "Ensure: Ensemble stein's unbiased risk estimator for unsupervised learning," in *ICASSP 2021-2021 IEEE International Conference on Acoustics, Speech and Signal Processing (ICASSP)*, pp. 1160–1164, IEEE, 2021.
- [31] G. Zeng, Y. Guo, J. Zhan, Z. Wang, Z. Lai, X. Du, X. Qu, and D. Guo, "A review on deep learning MRI reconstruction without fully sampled k-space," *BMC Medical Imaging*, vol. 21, no. 1, pp. 1–11, 2021.
- [32] J. Lehtinen, J. Munkberg, J. Hasselgren, S. Laine, T. Karras, M. Aittala, and T. Aila, "Noise2noise: Learning image restoration without clean data," *arXiv preprint arXiv:1803.04189*, 2018.
- [33] A. Krull, T.-O. Buchholz, and F. Jug, "Noise2void-learning denoising from single noisy images," in *Proceedings of the IEEE/CVF Conference on Computer Vision and Pattern Recognition*, pp. 2129–2137, 2019.
- [34] J. Batson and L. Royer, "Noise2self: Blind denoising by self-supervision," in *International Conference on Machine Learning*, pp. 524–533, PMLR, 2019.
- [35] N. Moran, D. Schmidt, Y. Zhong, and P. Coady, "Noisier2noise: Learning to denoise from unpaired noisy data," in *Proceedings of the IEEE/CVF Conference on Computer Vision and Pattern Recognition*, pp. 12064–12072, 2020.
- [36] Y. Xie, Z. Wang, and S. Ji, "Noise2same: Optimizing a self-supervised bound for image denoising," *Advances in Neural Information Processing Systems*, vol. 33, pp. 20320–20330, 2020.
- [37] A. A. Hendriksen, D. M. Pelt, and K. J. Batenburg, "Noise2inverse: Self-supervised deep convolutional denoising for tomography," *IEEE Transactions on Computational Imaging*, vol. 6, pp. 1320–1335, 2020.
- [38] K. Kim and J. C. Ye, "Noise2Score: Tweedie's Approach to Self-Supervised Image Denoising without Clean Images," *Advances in Neural Information Processing Systems*, vol. 34, 2021.
- [39] E. Kang, J. Min, and J. C. Ye, "A deep convolutional neural network using directional wavelets for low-dose X-ray CT reconstruction," *Medical physics*, vol. 44, no. 10, pp. e360–e375, 2017.
- [40] R. Flamary, "Astronomical image reconstruction with convolutional neural networks," in *2017 25th European Signal Processing Conference (EUSIPCO)*, pp. 2468–2472, 2017.
- [41] A. Sriram, J. Zbontar, T. Murrell, A. Defazio, C. L. Zitnick, N. Yakubova, F. Knoll, and P. Johnson, "End-to-end variational networks for accelerated MRI reconstruction," in *International Conference on Medical Image Computing and Computer-Assisted Intervention*, pp. 64–73, Springer, 2020.
- [42] O. Ronneberger, P. Fischer, and T. Brox, "U-net: Convolutional networks for biomedical image segmentation," in *International Conference on Medical Image Computing and Computer-Assisted Intervention*, pp. 234–241, Springer, 2015.
- [43] D. P. Kingma and J. Ba, "Adam: A method for stochastic optimization," *arXiv preprint arXiv:1412.6980*, 2014.
- [44] B. Yaman, S. A. H. Hosseini, S. Moeller, J. Ellermann, K. Uğurbil, and M. Akçakaya, "Multi-mask self-supervised learning for physics-guided neural networks in highly accelerated MRI," *arXiv preprint arXiv:2008.06029*, 2020.
- [45] Z. Wang, A. C. Bovik, H. R. Sheikh, and E. P. Simoncelli, "Image quality assessment: From error visibility to structural similarity," *IEEE Transactions on Image Processing*, vol. 13, no. 4, pp. 600–612, 2004.
- [46] M. Blumenthal, G. Luo, M. Schilling, M. Haltmeier, and M. Uecker, "NLINV-Net: Self-Supervised End-2-End Learning for Reconstructing Undersampled Radial Cardiac Real-Time Data," in *ISMRM annual meeting*, 2022.
- [47] A. D. Desai, B. M. Ozturkler, C. M. Sandino, S. Vasanawala, B. A. Hargreaves, C. M. Re, J. M. Pauly, and A. S. Chaudhari, "Noise2recon: A semi-supervised framework for joint MRI reconstruction and denoising," *arXiv preprint arXiv:2110.00075*, 2021.